The Astronomical Journal, 155:125 (7pp), 2018 March https://doi.org/10.3847/1538-3881/aaaa65

LHS 1610A: A Nearby Mid-M Dwarf with a Companion That Is Likely a Brown Dwarf

Jennifer G. Winters[1], Jonathan Irwin[1], Elisabeth R. Newton[2], David Charbonneau[1], David W. Latham[1], Eunkyu Han[3], Philip S. Muirhead[3], Perry Berlind[1], Michael L. Calkins[1], and Gil Esquerdo[1]
[1] Harvard-Smithsonian Center for Astrophysics, 60 Garden Street Cambridge, MA 02138, USA; jennifer.winters@cfa.harvard.edu
[2] Massachusetts Institute of Technology MIT Kavli Institute for Astrophysics and Space Research, 77 Massachusetts Avenue, Building 37-675 Cambridge, MA 02109, USA
[3] Department of Astronomy & The Institute for Astrophysical Research, Boston University, 725 Commonwealth Avenue, Boston, MA 02215, USA
Received 2017 December 7; revised 2018 January 19; accepted 2018 January 22; published 2018 February 23

Abstract

We present the spectroscopic orbit of LHS 1610A, a newly discovered single-lined spectroscopic binary with a trigonometric distance placing it at 9.9 ± 0.2 pc. We obtained spectra with the TRES instrument on the 1.5 m Tillinghast Reflector at the Fred Lawrence Whipple Observatory located on Mt. Hopkins in AZ. We demonstrate the use of the TiO molecular bands at 7065–7165 Å to measure radial velocities and achieve an average estimated velocity uncertainty of 28 m s^{-1}. We measure the orbital period to be 10.6 days and calculate a minimum mass of 44.8 ± 3.2 $M_{\rm Jup}$ for the secondary, indicating that it is likely a brown dwarf. We place an upper limit to 3σ of 2500 K on the effective temperature of the companion from infrared spectroscopic observations using IGRINS on the 4.3 m Discovery Channel Telescope. In addition, we present a new photometric rotation period of 84.3 days for the primary star using data from the MEarth-South Observatory, with which we show that the system does not eclipse.

Key words: binaries: spectroscopic – brown dwarfs – stars: low-mass – stars: rotation

Supporting material: data behind figure

1. Introduction

The nearest stars provide the best representatives of their kinds for study, with the canonical 10 pc sample containing the most easily targeted sample of stars. Remarkably, discoveries within this volume continue to be made, especially among the M dwarf population. New members of note include both M dwarf primaries and their stellar and sub-stellar companions, as reported in Deacon et al. (2005b), Biller et al. (2006), Henry et al. (2006), Winters et al. (2011), Davison et al. (2014).

In number, M dwarfs make up 75% of all stars (Henry et al. 2006), but have historically been challenging targets to study due to their low luminosities. This has been especially true in the field of high-resolution spectroscopy, which typically requires bright targets. Thus, many faint, nearby M dwarfs lack high-resolution spectroscopic measurements. However, the combination of modern echelle/CCD spectrographs with new analysis techniques allows this population of stars to benefit from higher-resolution instrumentation.

Multiplicity studies contribute to a better understanding of star and planet formation, as the shape of mass ratio distributions provides hints as to which pairs of stars are preferentially formed. Equal-mass (and therefore, equal-luminosity) companions are typically the most easily studied. Low-mass companions contribute very little light to the system and are therefore more challenging to detect. Companions that are both low-mass *and* members of short orbital period binaries can usually be detected only via the radial velocity method, as their corresponding angular separations are too small to resolve with other techniques such as astrometry, adaptive optics imaging, lucky imaging, or speckle interferometry. Because the mass ratio distribution for M dwarfs is not yet well measured at small mass ratios (where mass ratio $q = M_{\rm sec}/M_{\rm pri} < 0.50$ and where $M_{\rm pri}$ and $M_{\rm sec}$ represent the masses of the primary and secondary components, respectively), the identification and characterization of short-period low-mass companions, in particular, is critical to understanding the shape of the distribution. This can only be accomplished with high-resolution spectroscopic work.

While it has been shown that stellar companions are less common around M dwarfs than around more massive stars (Henry 1991; Fischer & Marcy 1992; Duchêne & Kraus 2013; Janson et al. 2014; Ward-Duong et al. 2015; Winters 2015), brown dwarf companions to M dwarfs are even more rare. Few examples are known, despite significant efforts to identify them in the solar neighborhood (Campbell et al. 1988; Marcy & Benitz 1989; Henry & McCarthy 1990; Tokovinin 1992; Dieterich et al. 2012). Only four M dwarf–brown dwarf pairs are known within 10 pc. Additions to this meager population provide precious data points to aid in constraining star and planet formation and evolution models.

We are conducting a multi-epoch spectroscopic survey of a volume-complete all-sky sample of 456 stars with estimated masses 0.1–0.3 $M_{\odot}$ and with trigonometric distances placing them within 15 pc. During the course of our observations, we discovered a previously unknown single-lined spectroscopic binary: LHS 1610A. We list the parameters for the system in Table 1. Here, we present the characterization of this system.

2. Data Acquisition

We obtained 13 optical spectra between UT 2017 February 1 and 2017 March 12 using the Tillinghast Reflector Echelle Spectrograph (TRES) on the FLWO 1.5 m Tillinghast Reflector. TRES is a high-throughput cross-dispersed fiber-fed echelle spectrograph. We used the medium fiber (2.″3 diameter) for a resolving power of $R \simeq 44{,}000$. The spectral resolution of the instrumental profile is 6.7 km s^{-1} at the center of all echelle orders. For calibration purposes, we acquired a thorium-argon lamp spectrum through the science fiber both

Table 1
System Parameters for LHS 1610A

Parameter	Value	References
R.A. (2000.0) (hh:mm:ss)	03:52:41.8	(2)
Decl. (2000.0) (dd:mm:ss)	+17:01:04	(2)
Proper Motion Mag. (mas yr^{-1})	767 ± 1.0	(2)
Proper Motion PA (deg)	146 ± 0.15	(2)
Parallax (mas)[a]	100.88 ± 2.05	(2), (4)
V_J (mag)	13.79 ± 0.02	(5)
R_{KC} (mag)	12.42 ± 0.02	(5)
I_{KC} (mag)	10.67 ± 0.02	(5)
J (mag)	8.93 ± 0.03	(3)
H (mag)	8.38 ± 0.03	(3)
K_S (mag)	8.05 ± 0.02	(3)
Primary mass ($M_\odot$)[b]	0.17 ± 0.02	(1)
Spectral Type	M4.0 V	(2)
Rotation Period (days)[c]	84.3	(1)
$U_\odot$ (km s^{-1})[d]	−30.5 ± 0.4	(1)
$V_\odot$ (km s^{-1})[d]	−32.0 ± 0.7	(1)
$W_\odot$ (km s^{-1})[d]	−21.3 ± 0.3	(1)

Notes.
[a] Weighted mean parallax.
[b] Estimated using the M_K mass–luminosity relation from Benedict et al. (2016).
[c] As reported in Irwin et al. (2011a), signal injection and recovery tests indicate that uncertainties on MEarth period measurements are 5%–10% for periods between 50 and 100 days.
[d] Space motions relative to the solar system.
References. (1) this work; (2) Henry et al. (2006), (3) Skrutskie et al. (2006), (4) van Altena et al. (1995), (5) Weis (1996).

before and after every science spectrum. Exposure times were 900 s in good conditions, achieving a signal-to-noise ratio (S/N) of 15 per pixel at 7150 Å (the pixel scale at this wavelength is 0.059 Å pix^{-1}). These exposure times were increased where necessary in poor conditions. The spectra were extracted and processed using the pipeline described in Buchhave et al. (2010).

3. Radial Velocities and Orbit Determination

We derived radial velocities using standard cross-correlation procedures based on the methods of Kurtz & Mink (1998). We used an observed template spectrum of Barnard's Star, a slowly rotating (130.4 days, Benedict et al. 1998) M4.0 dwarf (Kirkpatrick et al. 1991), which was obtained on UT 2011 April 15. We performed correlations using a wavelength range of 7065 to 7165 Å in order 41 of the spectrum, a region dominated by strong molecular features due to TiO in mid-type M stars (Irwin et al. 2011b).

We adopt a Barycentric radial velocity of −110.3 ± 0.5 km s^{-1} for Barnard's Star, derived from presently unpublished CfA Digital Speedometer (Latham et al. 2002) measurements spanning 17 years. Barnard's Star and LHS 1610A both have negligible rotational broadening at the resolution of the TRES spectra, so it was not necessary to apply any rotational broadening to the template spectrum prior to correlation. The radial velocities derived from this analysis are reported in Table 2.

The useful radial velocity information content of the TRES spectra gathered in our program for mid-M stars is dominated by the features in order 41. We find the velocities in the other orders have higher scatter, and including them does not improve the results significantly. It is therefore not appropriate to use the rms of the velocities in the individual orders to estimate the uncertainties in our adopted order, as this would result in an overestimate. Instead, we derive the radial velocity uncertainties during fitting (e.g., Gregory 2005). These internal model-dependent uncertainties are σ/h, where σ is the parameter from the MCMC analysis found in Table 3 and h is the cross-correlation, evaluated at the best-fitting velocity and normalized to a peak value of one, as defined in Tonry & Davis (1979), for each spectrum listed in Table 2. Total

Table 2
Radial Velocities of LHS 1610A

BJD[a] (days)	v_{rad}[b,c] (km s^{-1})	h[d]
2457785.7131	28.448	0.941
2457786.7850	32.365	0.940
2457787.6378	35.502	0.943
2457794.6483	22.514	0.948
2457795.7182	26.224	0.945
2457800.7416	44.533	0.935
2457806.6698	27.585	0.936
2457807.6875	31.293	0.903
2457808.6590	34.944	0.931
2457821.6194	43.586	0.933
2457822.6458	45.893	0.906
2457823.6552	40.479	0.860
2457824.6210	25.451	0.915

Notes.
[a] Barycentric Julian Date of mid-exposure, in the TDB time-system.
[b] Barycentric radial velocity.
[c] Internal model-dependent uncertainties on each velocity are σ/h, where σ is listed in Table 3 and h is the peak-normalized cross-correlation for each spectrum listed here.
[d] Peak-normalized cross-correlation.

Table 3
Orbital Elements for LHS 1610A

Parameter	Value
MCMC parameters	
$e \cos \omega$	0.00245 ± 0.00148
$e \sin \omega$	0.36941 ± 0.00093
T_0 (BJD)	2457781.739 ± 0.011
P (days)	10.5918 ± 0.0028
γ (km s^{-1})[a]	33.324 ± 0.018
K (km s^{-1})	12.527 ± 0.017
σ (km s^{-1})	0.0265 ± 0.0072
Derived parameters	
e	0.36942 ± 0.00093
ω (deg)	89.62 ± 0.23
T_{peri} (BJD)	2457781.734 ± 0.013
$a_1 \sin i$ (au)	0.011333 ± 0.000016
$f_1(M)$ ($M_\odot$)	0.0017311 ± 0.0000070
q_{min}	0.252 ± 0.011
a_{min} (au)	0.0563 ± 0.0020
$M_{2,min}$ ($M_\odot$)	0.0428 ± 0.0031
$M_{2,min}$ (M_{Jup})	44.8 ± 3.2

Note.
[a] The uncertainty on the systemic velocity γ does not include the systematic uncertainty of 0.5 km s^{-1} from the Barnard's Star template radial velocity.

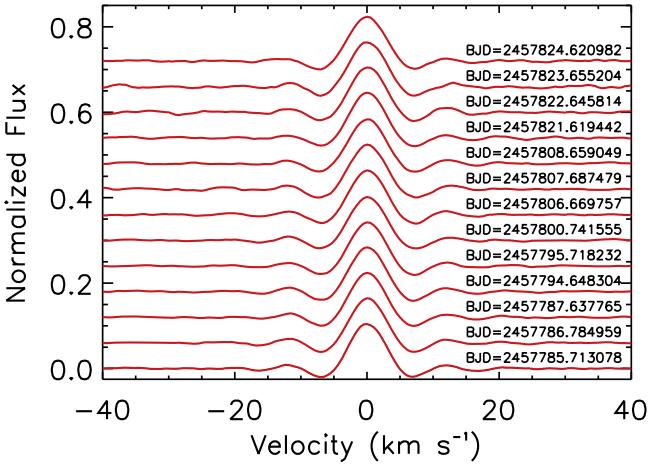

Figure 1. Least-Squares Deconvolution (LSD) curves for each spectrum, shifted to a velocity of zero and stacked for clarity. Noted is the Barycentric Julian Date for each observation. There is no evidence of a second spectrum due to a stellar companion in any of the LSDs, nor is there any rotational broadening.

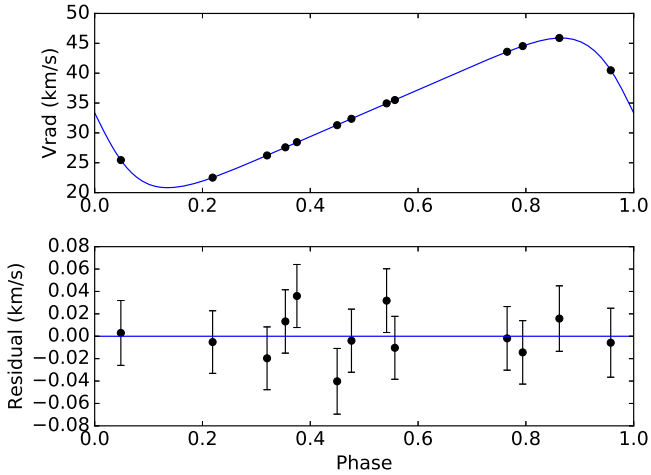

Figure 2. Spectroscopic orbit of LHS 1610A from TRES (upper panel) and residuals (lower panel) after subtracting the best-fitting model, plotted as a function of normalized orbital phase (measuring from 0 at inferior conjunction). The average estimated velocity uncertainty is 28 m s^{-1}.

uncertainties on each absolute measurement should include the systemic error of 0.5 km s^{-1} from the Barnard's Star template.

The cross-correlation functions (CCFs) we created using the TiO features in order 41, have a number of sidelobes surrounding the central peak. We find a pair of prominent local maxima at approximately $\pm$50 km s^{-1} from the central peak and numerous other features at larger velocities. These arise as a result of the structure of the molecular bandhead, with lines being close to evenly spaced in velocity. This does not affect the radial velocities determined from the cross-correlation peak, provided care is taken to fit only the central peak, but presents some difficulty for detection of additional stellar lines (e.g., due to additional components in multiple systems) and other conventional analysis of the correlation function such as line bisectors.

To alleviate this problem, we also perform a least-squares deconvolution (LSD) of the target star spectrum against the observed template spectrum (e.g., Donati et al. 1997). Deconvolution is prone to amplifying noise and producing spurious features, particularly in the present case where the template has the same resolution as the target. The target star spectra also tend to have low S/Ns (approximately 15, as noted above in Section 2), so we apply Tikhonov regularization (Tikhonov et al. 1998) and use features from several additional surrounding orders in the red part of the spectrum in this analysis to help with averaging out the noise.

We show the LSD curves for the individual epochs in Figure 1. As expected, these are compatible with δ-functions and show no indication of a second stellar spectrum due to a companion, nor any additional rotational broadening in LHS 1610A compared to Barnard's Star.

Having confirmed that the target is single-lined, we proceed to fit a standard eccentric Keplerian orbit to the velocities derived from the cross-correlation analysis using the EMCEE package (Foreman-Mackey et al. 2013) to implement a Markov Chain Monte Carlo (MCMC) sampler. This model has seven free parameters: the orbital period P, epoch of inferior conjunction T_0, e cos ω, e sin ω (where e is eccentricity and ω is argument of periastron), systemic radial velocity γ, semi-amplitude K and velocity uncertainty σ. We use e cos ω and e sin ω as jump parameters for mathematical convenience, but adopt uniform priors in e and ω. A modified Jeffreys prior of the form $1/(\sigma + \sigma_a)$ was used for σ with σ_a set to 10% of the final value determined for σ. In addition, we use the estimated primary mass as a jump parameter in order to propagate the uncertainty on the primary mass. We use a Gaussian prior on the primary mass with the mean and standard deviation fixed to the values reported in Table 1. Uniform improper priors were used for all other parameters. The individual data points were weighted by h^2 during fitting to account for the degradation of the velocity precision in epochs with lower peak correlation.

We ran simulations using 100 chains initialized using a Levenberg–Marquardt fit perturbed by 3σ using independent Gaussian deviates in each parameter. We ran chains for 6×10^4 samples, discarding the first 1×10^4 as a burn-in phase, resulting in a combined total of 5×10^6 samples from the posterior probability density function. We report the resulting parameters and uncertainties in Table 3 using the median and 68.3 percentile of the absolute deviation of the samples from the median as the central value and uncertainty, respectively. We show the orbit in Figure 2.

4. MEarth Photometric Rotation Period

As part of the characterization of this system, we present here a new photometric rotation period, measured using data from MEarth (Nutzman & Charbonneau 2008; Irwin et al. 2015). MEarth consists of eight robotic telescopes located atop Mt. Hopkins in Arizona (MEarth-North), and eight additional telescopes at the Cerro Tololo Inter-American Observatory (CTIO) in Chile (MEarth-South). To improve the determination of photometric rotation periods initially detected from MEarth-North, LHS 1610 was re-observed from MEarth-South to take advantage of the superior weather conditions at CTIO during the appropriate observing season for this object. We obtained data spanning a full observing season on 172 nights from UT 2016 August 4 to 2017 March 10 using a single telescope of the MEarth-South array. We acquired 3697 exposures of 15 s in groups of three back-to-back exposures, with these groups or "visits" to the target separated by approximately 30 minutes. Following our standard differential photometry procedures, we reduced the data to light curves, which we then analyzed as described in

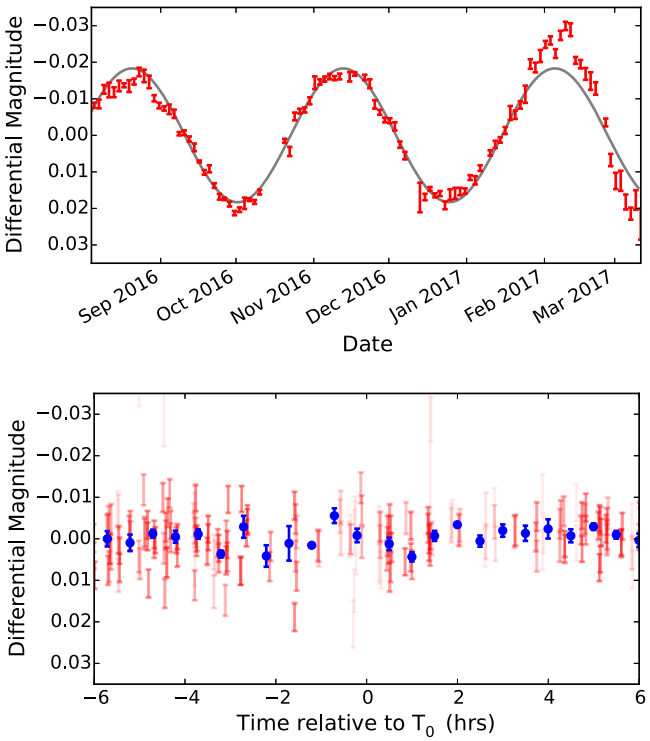

Figure 3. Top panel: light curve for LHS 1610A using data from MEarth-South, binned by 2 days. The gray line shows a model sinusoid, with a rotation period of 84.3 days and a variability semi-amplitude of 0.018 mag. Bottom panel: phase-folded residuals from the light curve (top panel), after removing a 2-day running median. Red points are the unbinned data from the top panel. The opacity of the points indicates the size of the error, with larger error points being more transparent. The blue points are the median of half-hour intervals. The error bars on the blue circles are the standard error on the mean, using 1.48× the median absolute deviation in place of the standard deviation. No eclipses are seen. The data used to create this figure are available.

Irwin et al. (2011a) and Newton et al. (2016). We show the resulting light curve in the top panel of Figure 3; the light curve data are listed in an electronic-only table.

From this analysis, we determine a rotation period of 84.3 days with a semi-amplitude of variability of 0.018 magnitudes. A small evolution of the morphology of the modulation is seen toward the end of the observing season. Our new period is consistent with our previous detection of an 83.7-day rotation period using MEarth-North data, as reported in Newton et al. (2016) and which was an update of the 78.8-day period reported in Irwin et al. (2011a). However, the new light curve contains denser sampling over two complete rotation cycles and is an improvement over our previous measurements. We assign this object a "grade A" rotation period on the scale defined in Newton et al. (2016).

The phase coverage of the photometry is also sufficient to search for eclipses. We look for a primary eclipse using the light curve from MEarth-South, shown in the top panel of Figure 3. To remove the stellar variability, which is not quite sinusoidal, we apply a running 2-day median filter. We then phase-folded the data using the period and ephemeris listed in Table 3. After rejecting outliers with absolute relative flux greater than 0.02 mag, we find the median absolute deviation is 0.0035 and 0.0017 for unbinned and binned data, respectively. As is shown in the bottom panel of Figure 3, no eclipses are present in the data.

5. Constraints on the Companion

5.1. Photometry and Astrometry

Because both good quality *VRIJHK* photometry and accurate trigonometric parallaxes exist for this object, we compare the photometric distance estimate, calculated using the distance relation in Henry et al. (2004), with the trigonometric distance to place upper limits on the mass of the secondary component. An equal-luminosity companion would result in the overluminosity of the system and its photometric distance estimate would therefore be underestimated by a factor of $\sqrt{2}$ when compared to its trigonometric distance. We find a photometric distance estimate of 9.7 ± 1.5 pc, in agreement with the trigonometric distance of 9.9 ± 0.2 pc. We can therefore infer that the companion is not of equal luminosity.

Companions with magnitude differences (Δmag) of 2.5 (flux ratios = 10) from their primaries are reliably detected using the TODCOR package (Zucker & Mazeh 1994). The TiO-bands that we use for analysis are effectively in the *I*-band, so we compare the M_I of LHS 1610A to that of two known late M dwarfs: 2MASS J2306-0502 (also known as TRAPPIST-1), an M7.5 V (Cruz et al. 2003) and SCR J1845-6357A, an M8.5 V (Henry et al. 2006). We note that SCR 1845-6357A is known to have a T dwarf companion, but this companion contributes a negligible amount of light in the *I*-band. The M_I of LHS 1610A, 2MASS J2306-0502, and SCR J1845-6357 are 10.68, 13.60, and 14.45 mag, respectively. The magnitude differences in *I* between LHS 1610A and the two late M dwarfs are larger than 2.5 mag, so it is not likely that we would have detected a companion of spectral type M7.5 V or M8.5 V in our optical spectra. However, the M_K of the three stars are 8.08, 9.79, and 10.50 mag, respectively, resulting in $\Delta\text{mag} < 2.5$, so it is possible that we could detect an M7.5 and M8.5 dwarf in infrared spectra; see Section 5.3.

5.2. Age Estimate

In order to use evolutionary models to estimate an upper limit on the mass of the companion, we require an estimate of the age of the system. Our systemic velocity determination permits the calculation of galactic space motions, relative to the local standard of rest, using the method outlined in Johnson & Soderblom (1987). We find velocities of -30.5 ± 0.5, -32.0 ± 0.8, and -21.3 ± 0.4 km s^{-1} for $U_\odot$, $V_\odot$, $W_\odot$, respectively, where $U_\odot$ is the radial component, positive in the direction of the Galactic center, $V_\odot$ is the azimuthal component, and $W_\odot$ is the vertical component. Using these space velocities and the method described in Bensby & Feltzing (2003), we calculate a probability of only 1% that the object belongs to the thick disk population, as opposed to the thin disk population. We therefore deem LHS 1610A a member of the thin disk population, to which Bensby & Feltzing (2003) assign an average age of 4.9 ± 2.8 Gyr. Using the rotation period-age relation from Newton et al. (2016), we also conclude, due to its long rotation period, that the system is likely at least 4.5 Gyr old. We note that because the two age estimates agree, the rotation period of the primary has not been affected by the presence and close proximity of the secondary.

With this age estimate, we perform a linear interpolation of the 1 and 5 Gyr COND03 evolutionary models (Baraffe et al. 2003) to estimate an upper limit on the mass and effective temperature of an object with an M_K of 10.50 mag (i.e., SCR J1845-6357A, as described above). For an object

with an age of 1 Gyr, this results in a maximum mass and effective temperature of 0.082 $M_{\odot}$ and 2436 K; for a 5 Gyr-old object, we calculate a maximum mass and effective temperature of 0.084 $M_{\odot}$ and 2444 K.

5.3. Infrared Spectroscopy

To place further constraints on the secondary component, we observed LHS 1610A using the Immersion GRating INfrared Spectrometer (IGRINS; Yuk et al. 2010) on the 4.3-meter Discovery Channel Telescope (DCT) in Happy Jack, Arizona, on the nights of UT 2017 September 25 and 26. IGRINS is a cross-dispersed, high-resolution ($R = \lambda/\Delta\lambda =$ 45,000) near-infrared spectrograph with a wavelength coverage of 1.45 to 2.5 μm, which obtains simultaneous observations in both the H and K bands (Yuk et al. 2010; Park et al. 2014; Mace et al. 2016a, 2016b). We calculated exposure times to achieve an S/N of approximately 150 per wavelength bin. We observed the A0 V telluric standard stars HR 8422 and HR 945 either immediately before or after and within 0.1 airmasses of LHS 1610A. We used the publicly available reduction pipeline for IGRINS (Lee 2015) to process the spectra and XTELLCOR_GENERAL (Vacca et al. 2003) to remove the telluric lines.

To measure the IGRINS radial velocities, we followed the method described in Han et al. (2017). We used the ephemeris from the TRES spectroscopic orbit to determine that the orbital phases for the system were 0.67 (night one) and 0.77 (night two), near the maximum radial velocity separation. We did not detect the signal of the secondary component in the IGRINS data.

To place an upper limit on the mass of the secondary component, we injected BT-Settl models (Allard et al. 2012) of objects with effective temperatures ranging from 2000 K to 3100 K (cool brown dwarfs to spectral type M4), into the IGRINS spectra. We injected each BT-Settl model at different RV shifts of the primary component, calculated based on a grid of masses that ranged from 0.17 $M_{\odot}$, corresponding to an equal-mass companion, to 0.042 $M_{\odot}$, the lower-mass limit determined by the TRES orbital solution. Before injection, we matched the resolution of BT-Settl models to that of the IGRINS data and added photon noise corresponding to the expected brightness of the putative secondary. We assumed the radii of the primary and secondary components to be 0.15 $R_{\odot}$ and 0.10 $R_{\odot}$, respectively. After injecting the secondary signal into the IGRINS spectrum, we cross-correlated the simulated LHS 1610A spectrum with the BT-Settl synthetic spectra and searched for the mass where the companion became undetectable.

We show the results of our injection and recovery analysis in Figure 4. Plotted is the effective temperature of the BT-Settl models that we used versus the simulated secondary masses. The color bar indicates the detection level, which corresponds to the height of the cross-correlation peak in terms of the standard deviation of the entire CCF. It is evident that the effective temperature has a larger effect on the detection than the mass. We place an upper limit of 2500 K to 3σ on the effective temperature of the companion that we could have detected with our IGRINS data. We therefore conclude that the companion is not likely to be an M dwarf.

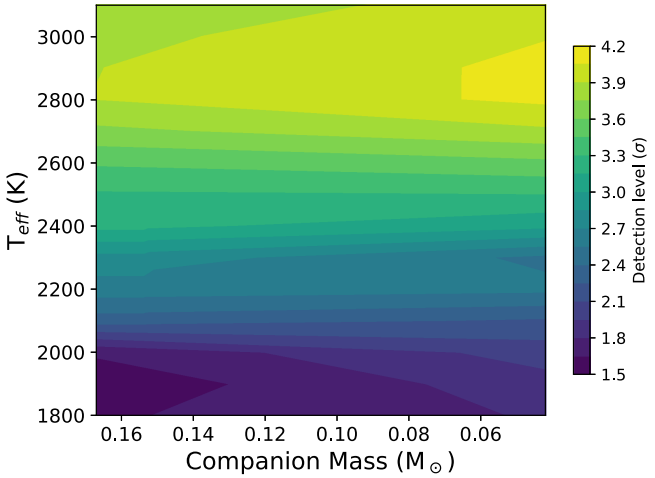

Figure 4. Illustrated is effective temperature vs. mass for LHS 1610B, with darker colors indicating a less significant detection. The results of our injection and recovery analysis indicate that we would have been able to detect to 3σ a companion at any mass with an effective temperature of roughly 2500 K, indicating that the companion is cooler than this temperature.

6. Discussion

LHS 1610 was noted as a double-lined spectroscopic binary in Bonfils et al. (2013). However, inspection of our initial TRES spectrum of this object did not reveal the second line indicative of a nearly equal luminosity stellar companion. We inspected the publicly available HARPS-GTO spectra of this object to determine whether our non-detection was due to the lower resolution of TRES, compared to that of HARPS, but did not see a second set of lines in those data. This object was not included in the sample of Tokovinin (1992), a work that searched for brown dwarf companions to M dwarfs, as the cooler spectral type limit of the sample was M3 V. As noted in Table 1, LHS 1610A has a spectral type of M4.0 V (Henry et al. 2006).

Preliminary work from Udry et al. (2000) showed for a small sample of M dwarf binaries that most systems with orbital periods of less than roughly 10 days have orbits that are nearly circular, similar to results for solar-type binaries (e.g., Duquennoy & Mayor 1991; Latham et al. 2002). Thus, with a 10.6-day orbit, the eccentricity of the system is not surprising, as its period is not short enough to have circularized.

We list the systems consisting of an M dwarf and a brown dwarf within 10 pc in Table 4. Of note is the scarcity of such systems: only four of the approximately 200 M dwarf systems within 10 pc (Henry et al. 2016) are known to harbor a brown dwarf companion. The primary component of GJ 229 is an early M dwarf, while GJ 569B, WIS J0720-0846A, and SCR J1845-6357A are all late M dwarfs. There are no reports of a mid-M dwarf within 10 pc in the literature with a confirmed brown dwarf companion. We do, however, note that there are two other nearby mid-M dwarfs suspected to have brown dwarf companions that have yet to be confirmed: GJ 595A (Nidever et al. 2002) and GJ 867B (Davison et al. 2015).

The range of mass ratios (0.50–0.25) for this system from the upper and lower mass limits (0.084–0.043 $M_{\odot}$) on the companion places it in a region of distribution space that is currently sparsely populated for M dwarfs (Winters 2015). We note that it is possible that the companion is an early L dwarf that lies above the hydrogen-burning limit of approximately

Table 4
Information for 10 pc MD+BD Systems

Name	R.A. (hh:mm:ss)	Decl. (dd:mm:ss)	d (pc)	References	a (au)	SpT_{pri}	SpT_{sec}	References	M_{pri} ($M_{\odot}$)
GJ 229AB	06:10:34.6	−21:51:52	5.8 ± 0.01	(10), (9), (6)	58	M1.5 V	T6	(4)	0.60 ± 0.02
WIS J0720-0846AB	07:20:03.3	−08:46:50	7.0 ± 0.02	(8)	1.2	M9.5 V	T5	(2)	0.075 ± 0.02
GJ 569BC	14:54:29.2	+16:06:03	9.9 ± 0.13	(10), (9)	0.9	M8.5 V	M9	(5)	$0.076^{+0.0086}_{-0.0076}$[a]
SCR J1845-6357AB	18:45:02.0	−63:57:47	3.9 ± 0.02	(3), (7)	5.7	M8.5 V	T6	(1)	0.075 ± 0.02
LHS 1610AB	03:52:41.0	+17:01:04	9.9 ± 0.2	(10), (7)	0.06	M4.0 V	⋯	(7)	0.17 ± 0.02

Note. Listed are the name of the pair, the epoch 2000.0 coordinates, the distance and error in parsecs, followed by the reference(s) for the parallax(es) from which the distance was calculated, and the projected linear separation in au. In the cases of GJ 229AB, WIS J0720-0846AB, and SCR J1845-6357AB, where no orbits exist, the calculated projected linear separation (angular separation × distance) has been multiplied by a factor of 1.26, as prescribed in Fischer & Marcy (1992). Next are listed the spectral types of the primary and secondary, along with the reference. Finally, the masses of the primary components are listed. These masses have been estimated using the M_K mass–luminosity relation from Benedict et al. (2016).

[a] GJ 569BC is the only pair with measured dynamical masses, for which Dupuy & Liu (2017) report $M_{pri} = 80^{+9}_{-8}\,M_{Jup}$ and $M_{sec} = 58^{+7}_{-9}\,M_{Jup}$.

References. (1) Biller et al. (2006), (2) Burgasser et al. (2015), (3) Deacon et al. (2005a), (4) Dieterich et al. (2012), (5) Dupuy & Liu (2017), (6) Gaia Collaboration et al. (2016), (7) Henry et al. (2006), (8) Scholz (2014), (9)van Leeuwen (2007), (10) van Altena et al. (1995).

2075 K (Dieterich et al. 2014). However, if we assume that the average value of $\sin^3 i$ is $3\pi/16$, then the mass is on average a factor of 1.7 larger than the minimum mass. This would result in a mass for the secondary of roughly 0.073 $M_{\odot}$, which is just at the 0.070–0.075 $M_{\odot}$ mass boundary between stars and brown dwarfs (Benedict et al. 2016; Dupuy & Liu 2017).

Future work will enable a better constraint on the secondary component of this system. For example, because the companion is unequal in both flux and mass, this system should exhibit an astrometric perturbation on the photocenter of the system (van de Kamp 1975). The magnitude of the perturbation, which we estimate to be approximately 7.5 mas, should be detectable by *Gaia*. An astrometric orbit from *Gaia* will provide the inclination for the system and permit the calculation of dynamical masses for the two components. Our TRES spectroscopic orbit will provide the necessary ephemeris for the astrometric orbital solution.

The authors thank the anonymous referee both for their prompt response and for their comments and suggestions. We thank Samuel Quinn, Guillermo Torres, Sergio Dieterich, Trent Dupuy, Wei-Chun Jao, Jayne Birkby, and Matthew Payne for illuminating discussions and suggestions. We especially thank Todd Henry for his assistance with the list of nearby M dwarf–brown dwarf binaries. We express our gratitude to Jessica Mink for the processing and extraction of the TRES spectra.

The MEarth Team gratefully acknowledges funding from the David and Lucille Packard Fellowship for Science and Engineering (awarded to D.C.). This material is based upon work supported by the National Science Foundation under grants AST-0807690, AST-1109468, AST-1004488 (Alan T. Waterman Award), and AST-1616624. E.R.N. is supported by an NSF Astronomy and Astrophysics Postdoctoral Fellowship. This publication was made possible through the support of a grant from the John Templeton Foundation. The opinions expressed in this publication are those of the authors and do not necessarily reflect the views of the John Templeton Foundation.

P.S.M. and E.H. acknowledge support from the NASA Exoplanet Research Program (XRP) under grant No. NNX15AG08G issued through the Science Mission Directorate.

These results made use of the Discovery Channel Telescope at Lowell Observatory, supported by Discovery Communications, Inc., Boston University, the University of Maryland, the University of Toledo and Northern Arizona University. This work used the Immersion Grating Infrared Spectrograph (IGRINS) that was developed under a collaboration between the University of Texas at Austin and the Korea Astronomy and Space Science Institute (KASI) with the financial support of the U.S. National Science Foundation under grant AST-1229522, of the University of Texas at Austin, and of the Korean GMT Project of KASI.

Facilities: FLWO:1.5m (TRES), DCT 4.3m (IGRINS).

ORCID iDs

Jennifer G. Winters https://orcid.org/0000-0001-6031-9513
Elisabeth R. Newton https://orcid.org/0000-0003-4150-841X
David Charbonneau https://orcid.org/0000-0002-9003-484X
David W. Latham https://orcid.org/0000-0001-9911-7388
Eunkyu Han https://orcid.org/0000-0001-9797-0019
Philip S. Muirhead https://orcid.org/0000-0002-0638-8822
Michael L. Calkins https://orcid.org/0000-0002-2830-5661

References

Allard, F., Homeier, D., & Freytag, B. 2012, RSPTA, 370, 2765
Baraffe, I., Chabrier, G., Barman, T. S., Allard, F., & Hauschildt, P. H. 2003, A&A, 402, 701
Benedict, G. F., Henry, T. J., Franz, O. G., et al. 2016, AJ, 152, 141
Benedict, G. F., McArthur, B., Nelan, E., et al. 1998, AJ, 116, 429
Bensby, T., Feltzing, S., & Lundström, I. 2003, A&A, 410, 527
Biller, B. A., Kasper, M., Close, L. M., Brandner, W., & Kellner, S. 2006, ApJL, 641, L141
Bonfils, X., Delfosse, X., Udry, S., et al. 2013, A&A, 549, A109
Buchhave, L. A., Bakos, G. Á, Hartman, J. D., et al. 2010, ApJ, 720, 1118
Burgasser, A. J., Gillon, M., Melis, C., et al. 2015, AJ, 149, 104
Campbell, B., Walker, G. A. H., & Yang, S. 1988, ApJ, 331, 902
Cruz, K. L., Reid, I. N., Liebert, J., Kirkpatrick, J. D., & Lowrance, P. J. 2003, AJ, 126, 2421
Davison, C. L., White, R. J., Henry, T. J., et al. 2015, AJ, 149, 106
Davison, C. L., White, R. J., Jao, W.-C., et al. 2014, AJ, 147, 26
Deacon, N. R., Hambly, N. C., & Cooke, J. A. 2005a, A&A, 435, 363
Deacon, N. R., Hambly, N. C., Henry, T. J., et al. 2005b, AJ, 129, 409
Dieterich, S. B., Henry, T. J., Golimowski, D. A., Krist, J. E., & Tanner, A. M. 2012, AJ, 144, 64
Dieterich, S. B., Henry, T. J., Jao, W.-C., et al. 2014, AJ, 147, 94
Donati, J.-F., Semel, M., Carter, B. D., Rees, D. E., & Collier Cameron, A. 1997, MNRAS, 291, 658
Duchêne, G., & Kraus, A. 2013, ARA&A, 51, 269
Dupuy, T. J., & Liu, M. C. 2017, ApJS, 231, 15
Duquennoy, A., & Mayor, M. 1991, A&A, 248, 485
Fischer, D. A., & Marcy, G. W. 1992, ApJ, 396, 178
Foreman-Mackey, D., Hogg, D. W., Lang, D., & Goodman, J. 2013, PASP, 125, 306

Gaia Collaboration, Brown, A. G. A., Vallenari, A., et al. 2016, A&A, 595, A2
Gregory, P. C. 2005, ApJ, 631, 1198
Han, E., Muirhead, P. S., Swift, J. J., et al. 2017, AJ, 154, 100
Henry, T. J. 1991, PhD thesis, Arizona Univ.
Henry, T. J., Jao, W.-C., Subasavage, J. P., et al. 2006, AJ, 132, 2360
Henry, T. J., Jao, W.-C., Winters, J. G., et al. 2016, in AAS Meeting 227 Abstracts, 142.01
Henry, T. J., & McCarthy, D. W., Jr. 1990, ApJ, 350, 334
Henry, T. J., Subasavage, J. P., Brown, M. A., et al. 2004, AJ, 128, 2460
Irwin, J., Berta, Z. K., Burke, C. J., et al. 2011a, ApJ, 727, 56
Irwin, J. M., Berta-Thompson, Z. K., Charbonneau, D., et al. 2015, 18th Cambridge Workshop on Cool Stars, Stellar Systems, and the Sun (Cambridge: Cambridge Univ. Press), 767
Irwin, J. M., Quinn, S. N., Berta, Z. K., et al. 2011b, ApJ, 742, 123
Janson, M., Bergfors, C., Brandner, W., et al. 2014, ApJ, 789, 102
Johnson, D. R. H., & Soderblom, D. R. 1987, AJ, 93, 864
Kirkpatrick, J. D., Henry, T. J., & McCarthy, D. W., Jr. 1991, ApJS, 77, 417
Kurtz, M. J., & Mink, D. J. 1998, PASP, 110, 934
Latham, D. W., Stefanik, R. P., Torres, G., et al. 2002, AJ, 124, 1144
Lee, J.-J. 2015, plp: Version 2.0, doi:https://doi.org/10.5281/zenodo.18579
Mace, G., Jaffe, D., Park, C., & Lee, J.-J. 2016a, 19th Cambridge Workshop on Cool Stars, Stellar Systems, and the Sun (Cambridge: Cambridge Univ. Press), 55
Mace, G., Kim, H., Jaffe, D. T., et al. 2016b, Proc. SPIE, 9908, 99080C
Marcy, G. W., & Benitz, K. J. 1989, ApJ, 344, 441
Newton, E. R., Irwin, J., Charbonneau, D., et al. 2016, ApJ, 821, 93
Nidever, D. L., Marcy, G. W., Butler, R. P., Fischer, D. A., & Vogt, S. S. 2002, ApJS, 141, 503
Nutzman, P., & Charbonneau, D. 2008, PASP, 120, 317
Park, C., Jaffe, D. T., Yuk, I.-S., et al. 2014, Proc. SPIE, 9147, 91471D
Scholz, R.-D. 2014, A&A, 561, A113
Skrutskie, M. F., Cutri, R. M., Stiening, R., et al. 2006, AJ, 131, 1163
Tikhonov, A., Leonov, A., & Yagola, A. 1998, Nonlinear Ill-Posed Problems (London: Chapman and Hall)
Tokovinin, A. A. 1992, A&A, 256, 121
Tonry, J., & Davis, M. 1979, AJ, 84, 1511
Udry, S., Mayor, M., Delfosse, X., Forveille, T., & Perrier-Bellet, C. 2000, IAU Symp. 200, Birth and Evolution of Binary Stars, (Cambridge: Cambridge Univ. Press), 158
Vacca, W. D., Cushing, M. C., & Rayner, J. T. 2003, PASP, 115, 389
van Altena, W. F., Lee, J. T., & Hoffleit, D. 1995, yCat, 1174, 0
van de Kamp, P. 1975, ARA&A, 13, 295
van Leeuwen, F. 2007, A&A, 474, 653
Ward-Duong, K., Patience, J., De Rosa, R. J., et al. 2015, MNRAS, 449, 2618
Weis, E. W. 1996, AJ, 112, 2300
Winters, J. G. 2015, PhD thesis, Georgia State Univ.
Winters, J. G., Henry, T. J., Jao, W.-C., et al. 2011, AJ, 141, 21
Yuk, I.-S., Jaffe, D. T., Barnes, S., et al. 2010, Proc. SPIE, 7735, 77351M
Zucker, S., & Mazeh, T. 1994, ApJ, 420, 806